Structural insights into the unusual core photocomplex from a triply extremophilic purple bacterium, Halorhodospira halochloris

Qi, Chen-Hui ; Wang, Guang-Lei ; Wang, Fang-Fang ; Wang, Jie ; Wang, Xiang-Ping ; Zou, Mei-Juan ; Ma, Fei ; Madigan, Michael T. ; Kimura,…

(Citation)
Journal of Integrative Plant Biology,66(10):2262-2272

(Issue Date)
2024-10

(Resource Type)
journal article

(Version)
Version of Record

JIPB Journal of Integrative Plant Biology

Research Article
https://doi.org/10.1111/jipb.13628

Structural insights into the unusual core photocomplex from a triply extremophilic purple bacterium, *Halorhodospira halochloris*

Chen-Hui Qi[1,2†], Guang-Lei Wang[1,2†], Fang-Fang Wang[3], Jie Wang[1,2], Xiang-Ping Wang[1,2], Mei-Juan Zou[1], Fei Ma[1], Michael T. Madigan[4], Yukihiro Kimura[5*], Zheng-Yu Wang-Otomo[6*] and Long-Jiang Yu[1*]

1. Key Laboratory of Photobiology, Photosynthesis Research Center, Institute of Botany, Chinese Academy of Sciences, Beijing 100093, China
2. University of Chinese Academy of Sciences, Beijing 100049, China
3. Zhangjiang Lab, National Facility for Protein Science in Shanghai, Shanghai Advanced Research Institute, Chinese Academy of Sciences, Shanghai 201210, China
4. Department of Microbiology, School of Biological Sciences, Southern Illinois University, Carbondale, IL 62901, USA
5. Department of Agrobioscience, Graduate School of Agricultural Science, Kobe University, Nada, Kobe 657-8501, Japan
6. Faculty of Science, Ibaraki University, Mito 310-8512, Japan

†These authors contributed equally to this work.

*Correspondences: Yukihiro Kimura (ykimura@people.kobe-u.ac.jp); Zheng-Yu Wang-Otomo (wang@ml.ibaraki.ac.jp); Long-Jiang Yu (longer@ibcas.ac.cn, Dr. Yu is fully responsible for the distributions of all materials associated with this article)

Chen-Hui Qi

Long-Jiang Yu

ABSTRACT

Halorhodospira (*Hlr.*) *halochloris* is a triply extremophilic phototrophic purple sulfur bacterium, as it is thermophilic, alkaliphilic, and extremely halophilic. The light-harvesting-reaction center (LH1–RC) core complex of this bacterium displays an LH1-Q_y transition at 1,016 nm, which is the lowest-energy wavelength absorption among all known phototrophs. Here we report the cryo-EM structure of the LH1–RC at 2.42 Å resolution. The LH1 complex forms a tricyclic ring structure composed of 16 αβγ-polypeptides and one αβ-heterodimer around the RC. From the cryo-EM density map, two previously unrecognized integral membrane proteins, referred to as protein G and protein Q, were identified. Both of these proteins are single transmembrane-spanning helices located between the LH1 ring and the RC L-subunit and are absent from the LH1–RC complexes of all other purple bacteria of which the structures have been determined so far. Besides bacteriochlorophyll *b* molecules (B1020) located on the periplasmic side of the *Hlr. halochloris* membrane, there are also two arrays of bacteriochlorophyll *b* molecules (B800 and B820) located on the cytoplasmic side. Only a single copy of a carotenoid (lycopene) was resolved in the *Hlr. halochloris* LH1–α3β3 and this was positioned within the complex. The potential quinone channel should be the space between the LH1–α3β3 that accommodates the single lycopene but does not contain a γ-polypeptide, B800 and B820. Our results provide a structural explanation for the unusual Q_y red shift and carotenoid absorption in the *Hlr. halochloris* spectrum and reveal new insights into photosynthetic mechanisms employed by a species that thrives under the harshest conditions of any phototrophic microorganism known.

Keywords: cryo-EM, LH1–RC, single carotenoid, three bacteriochlorophyll *b* molecules, triply extremophilic purple bacterium, unusual Q_y red shift

Qi, C.-H., Wang, G.-L., Wang, F.-F., Wang, J., Wang, X.-P., Zou, M.-J., Ma, F., Madigan, M.T., Kimura, Y., Wang-Otomo, Z.-Y., et al. (2024). Structural insights into the unusual core photocomplex from a triply extremophilic purple bacterium, *Halorhodospira halochloris*. J. Integr. Plant Biol. **00:** 1–11.

INTRODUCTION

Halorhodospira (*Hlr.*) *halochloris* is a physiologically remarkable bacteriochlorophyll (BChl) *b*-containing purple sulfur bacterium, which is a gammaproteobacterium and isolated from extremely saline soda lakes in Egypt (Imhoff and Trüper, 1977). The phototroph is a triple extremophile because of its halophilic, alkaliphilic, and thermophilic properties (Imhoff and Trüper, 1977; Imhoff and Suling, 1996). BChl *b*-containing phototrophic bacteria account for only a small fraction of all purple bacteria but possess unique photosynthetic properties in their ability to absorb near-infrared radiation above 1,000 nm (Kimura et al., 2021). Previous investigations indicate that *Hlr. halochloris* shows several striking photosynthetic features. For example, the Q_y transition of its light-harvesting 1 (LH) complex, which is intimately associated with the reaction center (RC) complex, absorbs at 1,016 nm, the lowest-energy wavelength known to support a phototrophic organism (Kimura et al., 2021). In addition, cells of *Hlr. halochloris* contain a photocomplex that absorbs at approximately 800 and 820 nm, which differs from absorption by typical LH2 complexes and other known LH complexes (Gardiner et al., 2020; Kimura et al., 2023; Liu et al., 2024; Swainsbury et al., 2023), suggesting that this organism contains binding sites for BChl *b* in addition to those found in other LH1 complexes and in the RC (Kimura et al., 2021). Furthermore, most LH1 complexes contain one or two carotenoids per α/β pair and one *cis*-carotenoid in the RC, but biochemical analysis showed that the *Hlr. halochloris* LH1–RC complex contains only a single lycopene molecule and is not located in the RC (Zhang et al., 2022), the typical location of such pigments; this suggests that in *Hlr. halochloris*, carotenoids may have other functions in addition to protecting photosynthetic machinery from excess light and as auxiliary light-harvesting pigments (Cogdell, 1985; Cogdell and Frank, 1987). Finally, sequence analysis has shown that the C-termini of the *Hlr. halochloris* LH1–αβ polypeptides contain significantly more acidic residues than do LH1–αβ polypeptides from their freshwater BChl *b*-containing counterparts, a structural modification that is likely related to the organism's unique halophilic biology (Imhoff and Trüper, 1977; Kimura et al., 2022).

Collectively, these unusual features make the *Hlr. halochloris* LH1–RC complex stand out among those of purple bacteria. Hence, its structural details could reveal new functional relationships that help define the physiochemical limits to photosynthesis. Currently, there is only one known structure of an LH1–RC complex containing BChl *b*, that being the complex from *Blastochloris* (*Blc.*) *viridis*, a freshwater phototroph that grows at neutral pH and at room temperature. However, the structure of this complex fails to explain the unique features of the *Hlr. halochloris* complex (Qian et al., 2018; Namoon et al., 2022; Hitchcock et al., 2023). Therefore, a more detailed picture of the *Hlr. halochloris* photocomplex structure and mechanism(s) controlling its LH1-Q_y red shift is necessary to truly understand photosynthetic light reactions in this organism. In this regard, here we present a cryogenic electron microscopy (cryo-EM) structure of the *Hlr. halochloris* LH1–RC complex. Our results provide the first structural foundation for the unique absorbance properties of *Hlr. halochloris* LH1, the position and function of the single carotenoid in the complex, and biochemical adaptations to life in a hot, alkaline and hypersaline environment. Further, our results point towards the direction for future investigations of light energy capture and transfer by this photosynthetically unique thermophilic, alkaliphilic, and halophilic phototroph.

RESULTS

Overall structure of the *Hlr. halochloris* LH1–RC complex

The cryo-EM structure of the LH1–RC complex from *Hlr. halochloris* was determined at 2.42 Å resolution (Figures 1A, S1–3; Table S1). The height of the core complex from the top of the periplasmic Cyt-subunit to the bottom of the cytoplasmic H-subunit is approximately 120 Å, and the diameter of the structure is also approximately 120 Å (Figure 1A). Due to the relatively long sequences of αβ polypeptides in the *Hlr. halochloris* complex compared with those in the LH1–RCs of other purple bacteria (Gardiner et al., 2020; Kimura et al., 2023; Liu et al., 2024; Swainsbury et al., 2023), the C-terminal loops form a 20-Å-high basin rim above the periplasmic side of the membrane (Figure 1A). Multiple genes encoding the LH1 α-, β- and γ-polypeptides were confirmed in the *Hlr. halochloris* genome (Figure S4). There are two forms of α-polypeptides, two forms of β-polypeptides, and one form of γ-polypeptide as identified from the density maps (Figure S1). The LH ring consists of 16 α1β1γ1 heterotrimers and one α3β3 heterodimer to form a tricyclic ring structure surrounding the RC (Figure 1A); the total number of polypeptides is similar to that of the *Blc. viridis* LH1 but the positions of the γ-polypeptide are different (Qian et al., 2018; Figure 1B). In order to clearly compare the LH1–RC complexes of *Blc. viridis* (Protein Data Bank (PDB) code: 6ET5) and *Hlr. halochloris*, the same chain ID was set according to that of *Blc. viridis*. The γ-polypeptide of *Hlr. halochloris* is located at the periphery of the β-polypeptide; by contrast, in *Blc. viridis*, the γ-polypeptide locates between neighboring β-polypeptides (Figure 1B). Interestingly, the position lacking the 17th γ-polypeptide in *Hlr. halochloris* LH1 also differs from that of *Blc. viridis* (Figure 1B); the N termini of the α- and β-polypeptides are on the cytoplasmic side, while the γ-polypeptide has an opposite topology, with its N terminus on the periplasmic side (Figure S1).

Spectrally, the *Hlr. halochloris* LH1–RC complex shows an LH1-Q_y absorption maximum at 1,016 nm with two additional bands at 797 and 818 nm, and shows an LH1-Q_y absorption maximum at 1,040 nm at 77 K (Zhang et al., 2022). In the LH1 structure, we found 17 pairs of BChl *b* (designated as B1020)

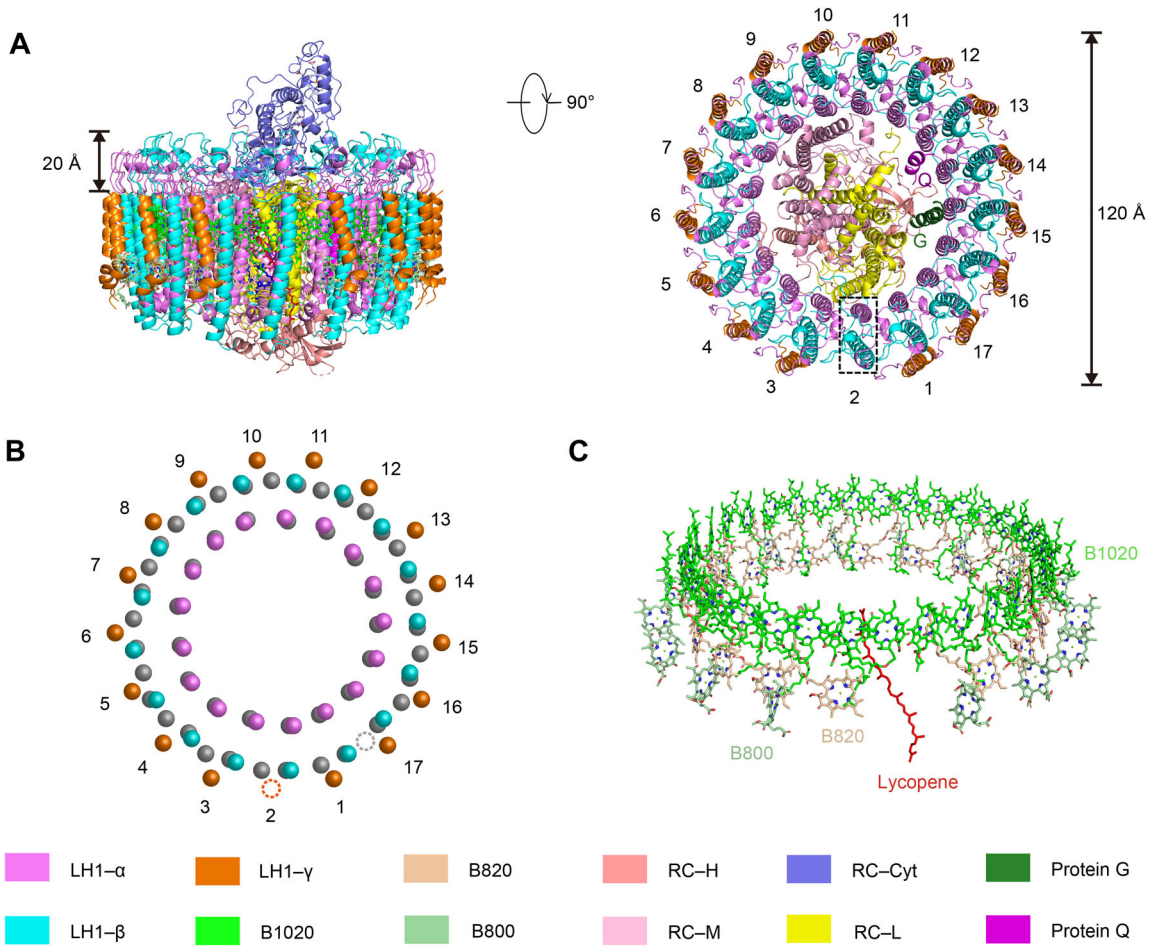

Figure 1. Overall structure of the LH1–RC complex from *Halorhodospira* (*Hlr.*) *halochloris*
(A) Cartoon representations of the LH1–RC complex are shown at side (left) or top (right) view. In the top view, pigments and the Cyt-subunit are omitted for clarity. The α3β3 pair is marked by a box. **(B)** Illustration of the relative arrangement of *Hlr. halochloris* and *Blastochloris* (*Blc.*) *viridis* (gray, PDB code: 6ET5) LH1 α-, β-, and γ-polypeptides shown with spheres. The absent γ-polypeptides of *Hlr. halochloris* and *Blc. viridis* are indicated by orange and gray dashed circles, respectively. **(C)** Tilted view of BChl *b* and the carotenoid in the LH1. The color code is shown below the panels.

on the periplasmic side of the membrane and a total of 32 BChl *b* molecules divided into two groups (designated as B820 and B800, respectively) on the cytoplasmic side (Figure 1C). Half of the BChl *b* molecules (B800 molecules) are inserted between adjacent β-subunits and are perpendicular to the membrane plane (Figure 2A); this differs from that of B800 from the LH2 of classical purple bacteria such as *Rhodobacter* (*Rba.*) *sphaeroides, Rhodoblastus acidophilus, Phaeospirillum molischianum*, and *Marichromatium purpuratum* that lie either parallel to the membrane plane (Prince et al., 2003; Qian et al., 2021c) or tilted away from the plane by up to 38° (Koepke et al., 1996; Gardiner et al., 2021). By contrast, the *Hlr. halochloris* B800 is similar to that of B800 from the aerobic purple bacterium *Gemmatimonas phototrophica* LH1–RC complex (Qian et al., 2022) with their bacteriochlorin rings lying perpendicular to those of the BChl *b* molecules that absorb at 820 nm (Figures 1C, 2A). In the α3β3 pair, not only is the γ-polypeptide absent but also B800 and B820, and thus the available space nicely accommodates the single lycopene, the only carotenoid molecule in the *Hlr. halochloris* LH1–RC complex (Figures 1C, 2A).

Unlike BChl *a* or *b* that is typically esterified with phytol or geranylgeraniol (Tani et al., 2021a; Qian et al., 2021b; Tani et al., 2021b), the BChl *b* of *Hlr. halochloris* contains a tetrahydrogeranylgeranyl (Δ2,10-phytadienyl) tail (Mizoguchi et al., 2009; Tsukatani et al., 2019; Hirose et al., 2022). In addition, in our study, two previously unrecognized proteins designated as proteins Q and G (to be described later) were discovered between the RC L-subunit and neighboring α-polypeptides in the *Hlr. halochloris* LH1–RC complex (Figure 1A); similar proteins have not been reported from the LH1–RC complexes of any other purple bacteria (Gardiner et al., 2020; Kimura et al., 2023; Liu et al., 2024; Swainsbury et al., 2023).

Arrangement of the LH1 multiple polypeptides and the single lycopene

Hlr. halochloris has four *pufA*, four *pufB*, and two γ-encoding genes in its annotated genome (GCF_002356555.2) (Figure S4), which is slightly different from the previous genome analysis (Tsukatani et al., 2019). Among these polypeptides, α2 and α4

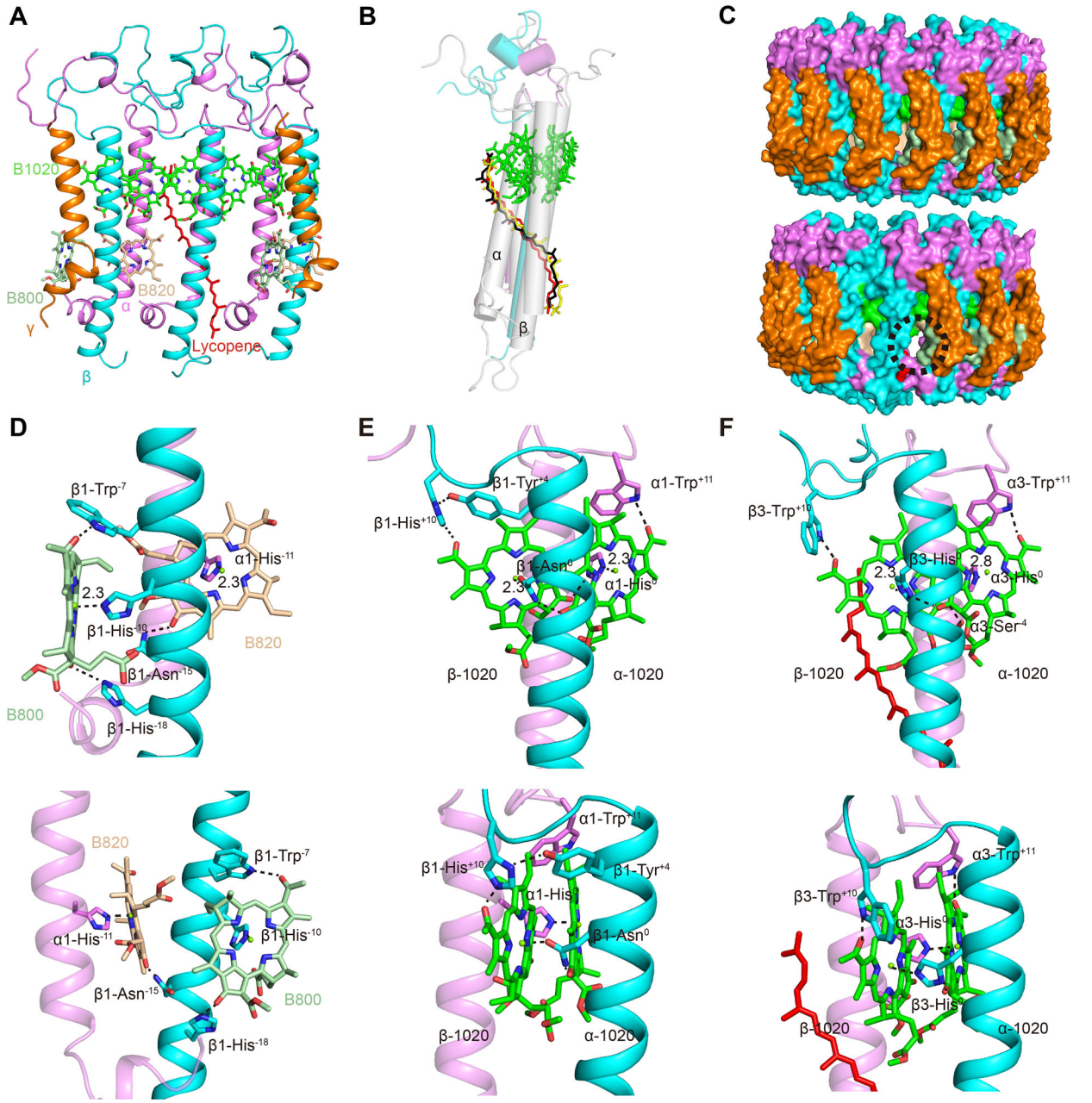

Figure 2. Structural details of the *Halorhodospira* (*Hlr.*) *halochloris* LH1 ring

(A) Side view of representative LH1 α1β1-polypeptides and α3β3-polypeptides. **(B)** The carotenoid in the *Hlr. halochloris* (red stick) in comparison with the carotenoids in the LH1 from *Blastochloris* (*Blc.*) *viridis* (black stick, PDB: 6ET5) and *Thermochromatium* (*Tch.*) *tepidum* (yellow stick, PDB: 5Y5S). LH1 αβ-polypeptides of *Hlr. halochloris* are respectively transparent violet and cyan cylinders and LH1 αβ-polypeptides between *Blc. viridis* and *Tch. tepidum* are transparent gray cylinders. **(C)** Side view of the surface representation shows a possible quinone channel due to absence of B820 and B800 from the α3β3-polypeptides in the *Hlr. halochloris* LH1–RC complex. The upper panel is a surface representation of the BChl blocking pore, and the lower panel is a surface representation of the pore formed by the α3β3-polypeptides where lycopene is located. The possible quinone channels are shown by black circles. **(D)** Hydrogen bonding of the cytoplasmic-side BChl of α1β1-polypeptides. Distance labels on the His-Mg chelation are shown. **(E)** Hydrogen bonding of periplasmic-side BChl of α1β1-polypeptides. **(F)** Hydrogen bonding of BChl of α3β3-polypeptides. The tail of BChl is omitted for clarity. **(D–F)** uses two angles to illustrate coordination or the hydrogen bonding interactions, respectively.

are identical while the α1 and α2 polypeptides differ only at positions +25 (aspartate for asparagine) and +30 (lysine for alanine) with the B1020 coordinating His residue defined as position 0 (Figure S4). By contrast, the sequences of α1/2/4 and α3 differ significantly (Figure S4). Based on their density, we identified 16 copies of α1 and one copy of α3 in the *Hlr. halochloris* LH1–RC (Figures 1A, S1). The situation with β-polypeptides is similar to that of α-polypeptides. β1/2/4 are slightly different only at their C-termini (Figure S4); however, these residues were not observed in the density map so it is unclear whether the mature protein actually contains them. As a result, the β1-polypeptides modeled in the LH1–RC structure

may also include β2 and/or β4, and so all β sequences in the model based on the density map are considered to be the same and are designated as β1. By contrast, the sequence of β3 not only differs from that of β1 but the polypeptide is also longer than that of β1 (Figure S4). There are two genes for the γ-polypeptide, with a substitution only at position +14 (leucine for methionine) in γ1 (Figure S4). The entire LH1 structure is composed of 16 heterotrimeric α1β1γ1 and one α3β3 pair, while the periphery of α3β3 contains no γ polypeptides (Figure 1A). By comparing amino acid sequences, it was revealed that α3 lacks the His^{-11} present in α1 that coordinates with Mg of B820, and that β3 lacks the His^{-10} of β1 that coordinates with Mg of B800 (Figure S5). As a result, unlike α1β1, the *Hlr. halochloris* LH1 composed of α3β3 is unable to bind B800 and B820 (Figure 2A).

The single lycopene molecule observed in the *Hlr. halochloris* LH1 complex is located on the LH1 formed by α3β3 where a γ-subunit is absent (Figure 1). This stoichiometry is consistent with the minimal absorbance at 450–550 nm in the spectrum (Zhang et al., 2022). As previously discussed, the unique amino acid sequences of α3 and β3 provide space for lycopene binding because these polypeptides lack coordinations to molecules of B800 and B820, respectively (Figures 2A, S5 and S6A). The position of the carotenoid in the *Hlr. halochloris* LH1 is similar to that in most LH1s reported so far (Gardiner et al., 2020; Kimura et al., 2023; Liu et al., 2024; Swainsbury et al., 2023), as shown by the comparison with representative *Thermochromatium* (*Tch.*) *tepidum* and *Blc. viridis* LH1s in Figure 2B. Although a carotenoid molecule is present, the absence of B800 and B820 forms a pore that provides a possible channel for quinone exchange to facilitate electron transport (Figure 2C).

Coordination of BChl *b* and γ-polypeptides in *Hlr. halochloris* LH1

Among the 16 *Hlr. halochloris* repeat LH1 units, we selected one pair to illustrate the binding mode of BChl *b* molecules (Figure 2D–E). From the results of amino acid sequence alignments of LH1 polypeptides from phototrophic bacteria, the amino acids that coordinate with the magnesium atom of bacteriochlorophylls are highly conserved histidines; however, the β-B1020 coordination in the *Hlr. halochloris* LH1 is different (Figures 2E, S5). In place of histidine, β-B1020 coordination in *Hlr. halochloris* is to asparagine (Figures 2E, S5). Asparagine coordination with chlorophyll is observed in the photosynthetic complexes of green plants, but this is the first observed instance of such coordination in a purple bacterial photocomplex. B1020 BChl coordinates with α1-His^0 and β1-Asn^0, the C3 acetyl group of α-B1020 forms a hydrogen bond with α-Trp^{+11}, and the $C13^1$ keto group forms a hydrogen bond with β1-Asn^0 (Figure 2E). In addition, β1-His^{+10} forms a hydrogen bond with the C3 acetyl group of β-B1020 and also with β1-Tyr^{+4} while the $C13^1$ keto group forms a hydrogen bond with α1-His^0 (Figure 2E). In the α3β3 pair, the Mg atoms of the two B1020 BChls coordinate with α3-His^0 and β3-His^0, respectively, while α3-Trp^{+11} and β3-Trp^{+10} form hydrogen bonds with the C3 acetyl group of α-B1020 and β-B1020, respectively (Figure 2F). In addition, α3-Ser^{-4} and β3-His^0 form hydrogen bonds with the C13 keto group of β-B1020 and α-B1020, respectively (Figure 2F).

The two BChl *b* molecules on the cytoplasmic side of the membrane are tentatively designated as B800 and B820, respectively. The Mg atom of the B820 molecule coordinates with α1-His^{-11} and its $C13^1$ keto group forms a hydrogen bond with nearby β1-Asn^{-15} (Figure 2D). The Mg atom of the B800 molecule coordinates with β1-His^{-10} and its C3 acetyl group forms a hydrogen bond with β1-Trp^{-7}; in addition, its $C13^1$ keto group forms a hydrogen bond with nearby β1-His^{-18} (Figure 2D). Moreover, two forms of BChl *b* were identified based on the high-resolution density (Figure S7A, B). B1020 and B820 are standard BChl *b* molecules with an ethylidene group on the same plane of bacteriochlorin, whereas B800 is 8-vinyl-BChl *b*, the major difference being whether the double bond is between C8-8^1 or $C8^1$-8^2 (Figure S7A). This modification allows the vinyl group to lie perpendicular to the bacteriochlorin ring (Figure S7B). HPLC analysis also showed that there were two major components of BChl molecules with a ratio of 3.5:1, and the Q_y transitions were at 795 and 777 nm, respectively, indicating that the latter one is actually a BChl *a* analogue with a single bond at C8-8^1 (Parkes-Loach et al., 1990; Canniffe and Hunter, 2014; Swainsbury et al., 2019; Saga et al., 2021) (Figure S8). In addition to the detection of both BChl *b* (Figure S8D, F), small amounts of carotenoids (Figure S8B) and oxidized BChl *b* (Figure S8C) were also found.

Unlike *Blc. viridis* LH1–RC in which the γ-polypeptides are sandwiched between neighboring β-polypeptides (Qian et al., 2018), the γ-polypeptides of *Hlr. halochloris* are located at the periphery of β-polypeptides. The γ-polypeptide is a transmembrane helix that interacts with the neighboring β1-polypeptide mainly by hydrophobic interactions, and additionally, Ala^{+15} of the γ-polypeptide forms a hydrogen bond with Ser^{-6} of the β1-polypeptide and γ-Asp^{+3} forms hydrogen bonds with Ile^{+28} and Trp^{+29} in the C-terminal loop region of the α1-polypeptide, respectively, facilitating the stabilization of the core complex by the γ-polypeptide (Figure S6B).

Unique features of the *Hlr. halochloris* RC complex

The L- and M-subunits of the *Hlr. halochloris* RC each consists of five transmembrane helices and forms a heterodimer that binds a BChl *b* dimer, two BChl *b* monomers, two BPhe *b* monomers, a non-heme iron, and one molecule each of UQ8 and MQ8. The overall structure of the *Hlr. halochloris* RC approximates that of the *Blc. viridis* RC complex (PDB code: 6ET5) (the root mean square deviation (r.m.s.d.) values of 1.59) (Figure 3A), with a major exception being the Cyt-subunit (Figure 3B, C). The basic and acidic residues in the Cyt-subunit of *Blc. viridis* are 41 and 28, respectively, whereas the corresponding number of residues from *Hlr. halochloris* is 31 and 68 (Figure S9C). Hence, the content of acidic residues in the *Hlr. halochloris* Cyt-subunit is more than twice that of the *Blc. viridis* Cyt-subunit. In addition, the content of acidic residues in the *Hlr. halochloris* LH1–RC

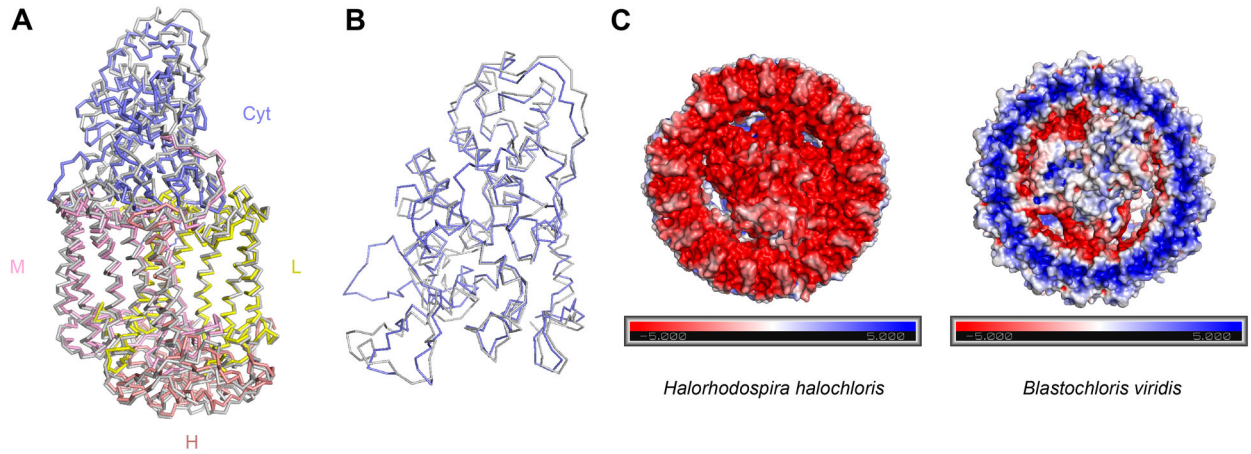

Figure 3. Structure characteristics of the Cyt-subunit in the *Halorhodospira* (*Hlr.*) *halochloris* RC
(A) Superposition of the RC of *Hlr. halochloris* and *Blastochloris* (*Blc.*) *viridis* (gray, PDB code: 6ET5). The colors of *Hlr. halochloris* RC polypeptides are the same as in Figure 1. **(B)** Alignment of the Cyt-subunits without heme groups of *Hlr. halochloris* and *Blc. viridis* (gray, PDB code: 6ET5). **(C)** Top view of surface charge distributions of the LH1–RC complexes from *Hlr. halochloris* and *Blc. viridis* with color codes according to the electrostatic potential from −5.0 kBT (red, negative charge) to +5.0 kBT (blue, positive charge) in the scale bars.

complex at the periplasmic surface is significantly higher than that of *Blc. viridis* and other purple bacteria (Figures 3C, S9A).

Proteins G and Q in the *Hlr. halochloris* RC complex

Two helical densities were clearly resolved in the *Hlr. halochloris* LH1–RC structure and were located between the L-subunit and the 13th and 15th α-polypeptide (Figure 4A). Small polypeptides such as these are located around the RC complex in some other purple bacteria—such as protein-U (elsewhere named as PufY or protein Y) and PufX in *Rba. sphaeroides* (Qian et al., 2021a; Tani et al., 2021b; Qian et al., 2021d; Cao et al., 2022; Tani et al., 2022) and protein h in *Roseiflexus (Rfl.) castenholzii* (Xin et al., 2018; Qi et al., 2023; Xin et al., 2023)—and are known to perform specific functions. However, the positions of these proteins differ from those of the small proteins in the *Hlr. halochloris* RC complex. Due to the encircling of the LH1 complex, the interior resolution was sufficient to trace most of the residues of these two previously unreported proteins, designated as proteins G and Q (Figure 4B). However, the genes were not annotated and had to be located manually. The genes encoding these two polypeptides were identified in the *Hlr. halochloris* DSM 1059^{T} genome (Tsukatani et al., 2019) and the proteins themselves were confirmed by liquid chromatography-tandem mass spectrometry (Figure S10). Each of these two integral membrane proteins contained a single helical conformation and had their N- and C-termini on the periplasmic and cytoplasmic sides, respectively (Figure 4B). Transmembrane proteins G and Q, contained highly hydrophobic residues rich in Ala, Val and Leu (Figure S10) and their structures were consistent with predictions from the membrane protein topology program TMHMM (Krogh et al., 2001) (Figure S11**)**. In addition, we found that Trp^{+28} and Trp^{+29} of protein Q form hydrogen bonds with Ala^{+2} of the M-subunit as well as Arg^{+30} of protein Q with Arg^{+215} of the H-subunit on the cytoplasmic side, respectively, and Gly^{+3} and Glu^{+4} of protein Q form hydrogen bonds with Arg^{+27} of the Cyt-subunit, respectively, as well as Thr^{+2} of protein Q forms hydrogen bonds with α1-Ser^{+5} on the periplasmic side (Figure S12A). As for protein G, we found that Arg^{+33} of protein G formed hydrogen bonds with Asp^{+155} and Asp^{+156} of the H-subunit, respectively, as well as with α1-Asp^{-20} for Arg^{+31} of protein G on the cytoplasmic side, and with α1-Glu^{+13} for Met^{+5} of protein G on the periplasmic side (Figure S12B). The gene encoding protein Q is located adjacent to genes in the *Hlr. halochloris* genome encoding threonylcarbamoyl-AMP synthase (WP_096409939.1), and the gene encoding protein G is located just downstream of that encoding protein Q (Figure 4C). At present, the function of proteins G and Q is unknown, but they are likely specific to the unusual halophilic phenotype of *Hlr. halochloris* since homologues of them were not detected in the RC of the freshwater BChl *b*-containing *Blc. viridis*.

DISCUSSION

Hlr. halochloris stands apart from all known phototrophic organisms for several reasons but in particular because its photosynthetic machinery absorbs the lowest-energy wavelengths of any known phototroph. There are at least five factors that may contribute to this unusual capacity. First is the inherent structural property of BChl *b* itself (Davis et al., 1996). BChl *b* exhibits a more red-shifted Q_y absorption than BChl *a* even when dissolved in organic solvents; for example, in acetone, the Q_y absorption of BChl *b* is at 791 nm and that of BChl *a* at 773 nm (Blankenship, 2021). Second, the coordination and hydrogen bonding between BChl *b* and LH1 polypeptides also contribute to the red shift. As described earlier, the Mg of *Hlr. halochloris* B1020 is coordinated with β1-Asn^{0} (or β3-His^{0}) and α1-His^{0} (or α3-His^{0}) (Figure 2E, F), respectively. Although the histidines are highly conserved, the

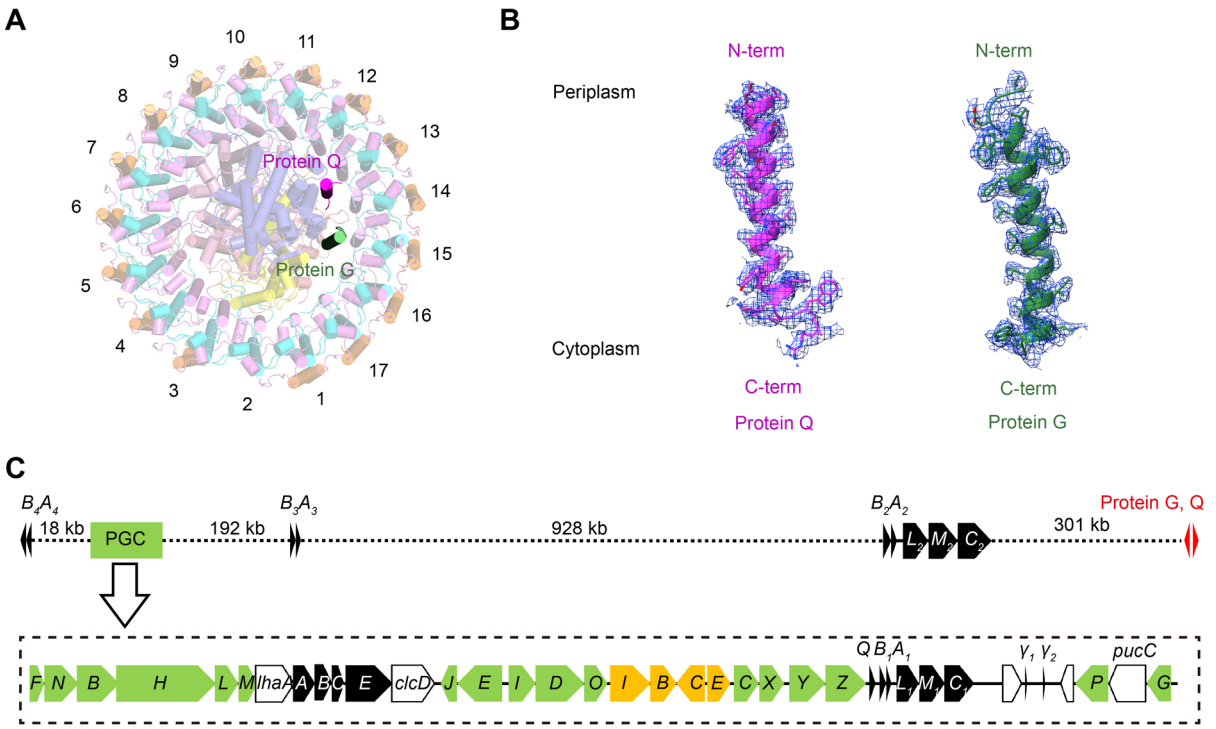

Figure 4. Identification of the two small polypeptides G and Q in the LH1–RC complex of *Halorhodospira* (*Hlr.*) *halochloris*
(A) Relative positions of protein Q and protein G in the LH1–RC complex. All proteins are shown by cylinders with the same color scheme as in Figure 1. **(B)** Cryo-EM densities and structural models of protein Q and protein G. **(C)** Arrangement of genes in the PGC and LH1–RC related genes in *Hlr. halochloris* genome. Genes are represented by rectangles pointing in the direction of transcription. Genes for bacteriochlorophyll (bch) and carotenoid biosynthesis are shown in green and orange, respectively. The *puf* and *puh* genes encoding the LH1–RC complex and related products are shown in black. Proteins Q and G are shown in red. Open reading frames without an assigned gene name are annotated as hypothetical proteins.

Hlr. halochloris β1-Asn^{0} is unique to this species and is found as a histidine in all other purple bacteria (Gardiner et al., 2020; Kimura et al., 2023; Liu et al., 2024; Swainsbury et al., 2023), including *Blc. viridis* (Figure S5). In plants, this asparagine–chlorophyll coordination is proposed to contribute to the red-shifted Q_y transition in LHCI of the photosystem I complex (Morosinotto et al., 2003). β1-Asn^{0} acts as an axial ligand of BChl *b* and by analogy, likely contributes to the unusual red shift of LH1-Q_y in *Hlr. halochloris*. Third, the extension of the *Hlr. halochloris* C-terminal loop regions of LH1 β-polypeptides could affect the Q_y transition as can be seen from the amino acid sequence and the modeled structure of the β-polypeptide, which has a longer C-terminal region than that of most purple bacterial β-polypeptides (Figure 1A). The polar C-terminal extensions of the α- and β-polypeptides of LH1 are also uniformly aligned by their electrostatic interactions to form a rigid structure, and this could also be an important factor influencing the unusual red shift of LH1-Q_y. Fourth, the *Hlr. halochloris* LH1 α-polypeptide has a unique cysteine residue (α1-Cys^{+3}) (corresponding to α-Leu^{+3} in *Blc. viridis* LH1), and both of these are positioned in the vicinity of the pyrrole of BChl *b* (Figure S7C). Under the alkaline conditions required for the growth of *Hlr. halochloris*, α1-Cys^{+3} thiol groups would be deprotonated, and the thiolate anion formed may also contribute to the red shift of LH1-Q_y. And finally, the presence of γ-polypeptides stabilizes the core complex, and their absence in *Blc. viridis* LH1 has been shown to cause a significant blue shift of the Q_y of the LH1–RC complex (Namoon et al., 2022).

Based on the different structures of LH1 that have been determined thus far as well as several amino acid sequence comparisons, it is known that the histidine residues that bind BChl molecules responsible for the Q_y absorption are highly conserved. However, in *Hlr. halochloris*, the histidines that coordinate B800 and B820 are not conserved in other phototrophic bacteria (Figure S5), which explains the specificity of B800 and B820 in the LH1 of *Hlr. halochloris*. Interestingly, β1-His^{-18} that binds the C13^{1} keto group of B800 is highly conserved (Figures 2D, S5), but with the exception of the filamentous phototroph *Rfl. castenholzii*, other phototrophic bacteria that have this conserved β-His^{-18} residue do not contain B800. β-His^{-18} that binds Mg of B800 (Xin et al., 2018; Qi et al., 2023; Xin et al., 2023) of *Rfl. castenholzii* and β1-His^{-18} that bind the C13^{1} keto group of B800 of *Hlr. halochloris* suggests that conserved β-His^{-18} coordinated BChl molecules gradually disappeared during the evolution of purple phototrophic bacteria resulting in the absence of B800 in other phototrophic LH1 complexes (Gardiner et al., 2020; Kimura et al., 2023; Liu et al., 2024; Swainsbury et al., 2023). This specificity of B800 and B820 leads to steric hindrance that occupies the space that would otherwise be taken by carotenoids (Figure S6A), explaining the low carotenoid content of the *Hlr. halochloris* complex. The *Hlr. halochloris* LH1 complex binds only one

carotenoid molecule that has been identified as an *all-trans* lycopene molecule (Zhang et al., 2022). In the cryo-EM structure of *Hlr. halochloris*, we located this lycopene molecule in the α3β3 subunit of the LH1 ring, a location similar to that reported from *Tch. tepidum* (Yu et al., 2018) (Figure 2B).

Two small RC proteins Q and G were discovered in this study. These two polypeptides have not been found in any purple bacterial RC complexes thus far and are encoded in the *Hlr. halochloris* genome at some distance from the photosynthetic gene cluster (Figure 4C), suggesting that they may not play a direct role in photosynthesis. However, from their positions in the LH1–RC complex, it is possible that proteins G and Q function as "spacers" to keep photosynthetically functional proteins positioned at specific locations to ensure their proper functioning.

Finally, we found that the *Hlr. halochloris* LH1–RC complex has a significantly higher acidic amino acid content on the periplasmic side than that of other phototrophic bacteria (Figures 3C, S9A). This is mainly due to the large number of acidic amino acid residues in its Cyt subunit (Figure S9C) and the fact that the α- and β-polypeptides also contain acidic amino acid residues at their C-termini (Figure S4). However, the charge distribution of the *Hlr. halochloris* LH1–RC complex on the cytoplasmic side is similar to that of *Blc. viridis* (Figure S9B), which means the intracellular physiological environment of cells of these bacteria are similar. By contrast, the large content of acidic amino acids on the periplasmic side of the *Hlr. halochloris* LH1–RC complex is undoubtedly a response to the high salinity and alkalinity of its habitat; in laboratory culture, the organism grows in medium saturated in NaCl at pH 10 (Imhoff and Trüper, 1977).

MATERIALS AND METHODS

Protein purification of the LH1–RC complex

Hlr. halochloris DSM 1059^T cells were grown phototrophically (anoxic/light) under incandescent light (40 W) for 7 days and harvested by centrifugation for 15 min at 9,954 *g* (Avanti J-26S XPI Centrifuge; Beckman Coulter, Palo Alto, CA, USA). Cells were collected, resuspended in 20 mM Tris-HCl buffer (pH 8.5), followed by ultrasonic disruption (Ultrasonic Homogenizer JY92-IIN; Scentz, Ningbo, China), then centrifuged at 27,216 *g* for 15 min, and the supernatant ultracentrifuged at 208,429 *g* for 1 h (Optima™ L-100 XP Ultracentrifuge; Beckman Coulter, USA). The chromatophores obtained were solubilized with 1% (w/v) *n*-octyl-β-D-glucoside (OG) for 1 h at room temperature and then ultracentrifuged at 208,429 *g* for 1 h. The obtained supernatant enriched with LH1–RC complex was loaded onto a DEAE column (Toyopearl 650S; Tosoh, Tokyo, Japan), equilibrated with 20 mM Tris-HCl buffer (pH 8.5) containing 0.03% (w/v) *n*-dodecyl β-D-maltopyranoside (DDM), and eluted with a linear gradient from 100 to 350 mM NaCl to collect fractions with a ratio of $A_{1016}/A_{280} > 0.8$ for cryo-EM data collection.

Pigments analysis

Pigments of the *Hlr. halochloris* LH1–RC complex were extracted with acetone-methanol (9:1, v/v) and then analyzed by HPLC on a C18 reversed-phase column (TSKgel Super-ODS, 4.6 mm×10 cm, particle size 2.3 μm) in a Waters2545Q with the recording wavelength range of 300–800 nm. The pigments were eluted with a flow rate of 0.6 mL/min using solvent A (90% methanol) for the first 4 min, followed by a constant solvent B (90% acetonitrile) until the end of the separation. Pigments were detected by their absorbance at 780 nm. The column was re-equilibrated in solvent A for 10 min prior to the next injection.

Cryo-EM data collection

The protein concentration was concentrated to an OD_{1016} of ~30. Three microliters of protein solution were applied to a glow-discharged (Solarus plasma cleaner; Gatan, Pleasanton, CA, USA) holey carbon grid (Quantifoil grid R2/1, 200 mesh Cu) that had been treated with H_2 and O_2 mixtures for 30 s. The grid was plunged into liquid ethane cooled by liquid nitrogen using Vitrobot Mark IV (Thermo Fisher Scientific, Hillsboro, OR, USA). The parameters were set as follows: blot force -1, blotting time 2 s, humidity 100%, sample chamber temperature 8°C. Data were collected on a Titan Krios (Thermo Fisher Scientific, Hillsboro, OR, USA) electron microscope at 300 kV equipped with a K2 camera (Gatan, Pleasanton, CA, USA), at a nominal magnification of 22.5 k in super-resolution mode. Movies were recorded in super-resolution mode and Fourier-cropped to give a resulting calibrated pixel size of 1.02 Å at the specimen level. An exposure rate of 8 e^- per pixel per s was set and a fresh super-resolution gain reference was performed at this dose rate before data acquisition. A total dose of 60.8 e^- per $Å^2$ was used for movies of 38 frames. In total, 2,160 movies for LH1–RC complex were collected with defocus values from –1.0 to –3.0 μm.

Image processing of the *Hlr. halochloris* LH1–RC complex

All frames Motion Correction and CTF Estimation were performed with CryoSPARC (Punjani et al., 2017). F-crop factor was set to ½ to generate aligned micrographs in Motion Correction. Particles were picked by crYOLO (Wagner and Raunser, 2020) using a pre-trained model. A total of 514,261 particles were picked from 2,160 micrographs at 0.1 threshold and 200-pixel box size. These particles were then imported to CryoSPARC at 360-pixel box size for 2D classification with 100 classes. Here, 412,594 particles were selected for a secondary 2D classification with 50 classes and 379,864 particles from 16 good classes were selected for 3D reconstruction. These particles were subjected to 3D Ab-Initio reconstruction of CryoSPARC to build four initial models. Two classes containing 353,518 particles were merged to execute Non-Uniform Refinement (Punjani et al., 2020; Zivanov et al., 2020). This resulted in a map at a global resolution of 2.42 Å.

Model building and refinement of the *Hlr. halochloris* LH1–RC complex

To build an atomic model, protein sequences of known subunits were submitted to SWISS-MODEL (Waterhouse et al., 2018), with the atomic model of *Tch. tepidum* LH1–RC complex (PDB: 5Y5S) (Yu et al., 2018) as a reference. The initial atomic model was manually checked to fit in the map, and unidentified subunits were modeled in COOT (Emsley et al., 2010). Realspace refinement was performed in PHENIX (Adams et al., 2011), and the COOT/PHENIX refinements were iterated until they converged. Finally, all parameters were generated by PHENIX. Figures were drawn with the PyMOL Molecular Graphic System (Schrödinger) (DeLano, 2004), UCSF Chimera (Pettersen et al., 2004) and UCSF ChimeraX (Pettersen et al., 2021).

Liquid chromatography-tandem mass spectrometry (LC–MS/MS) analysis

First, 1 mg/mL of *Hlr. halochloris* LH1–RC complex was desalted with Zip Tip C4, then it was dissolved in buffer A (ddH_2O containing 0.1% [v/v] formic acid) and manually sampled into the reverse phase C18 column (C18 material of 1.9 μm particle size was filled into a 25 cm length column with an internal diameter of 150 μm; Dr. Maisch GmbH Inc., Germany). It was connected to the Easy nLC-1200 for LC–MS/MS analysis using an Orbitrap Fusion Lumos ultra-high-resolution combined liquid mass spectrometer (Thermo Fisher Scientific, Waltham, MA, USA). The elution gradient was 30%–100% buffer B (0.1% [v/v] formic acid and 20% [v/v] water in acetonitrile) for 30 min and continued with 100% B for 40 min at a flow rate of 600 nL/min. The Orbitrap Fusion Lumos mass spectrometer MS1 parameters were Orbitrap resolution of 120 K, scan range of 350–1,550 *m/z*, automated gain control (AGC) target of 4E5, and include charge state of 3–10 s. In MS2, the activation type was higher energy collision dissociation (HCD), and HCD collision energy was 32%. Orbitrap resolution was 15,000, and the AGC target was set to 5E4 for analysis. The experiment was performed three times under each condition.

Data analysis

The full protein sequences of *Hlr. halochloris* from the National Center for Biotechnology Information (NCBI) and additional sequences of protein Q and protein G obtained in the translated genome were used to make a new database. The MS data obtained by topdown were converted to Mascot generic format (MGF) and searched in the resulting new database, Mascot 2.5.1.3 (Matrix Science) using a peptide tolerance of 10 ppm and an MS/MS tolerance of 0.6 Da, and the instrument was selected for the b-y ion, and peptides obtained from the search were considered to be present when the Mascot score was >20 and the expectation value was <0.05.

Data availability statement

The cryo-EM density maps were deposited in the Electron Microscopy Data Bank (EMDB, www.ebi.ac.uk/pdbe/emdb/) under the following accession code: EMD-36907 for the *Hlr. halochloris* LH1–RC complex. The atomic coordinates have been deposited in the Protein Data Bank (PDB, www.rcsb.org) under the following accession code: 8K5O. All other data are available from the corresponding authors upon reasonable request.

ACKNOWLEDGEMENTS

We thank Dr. Zhuang Lu from the Plant Science Facility, Dr. Qingtao Lu from the Photosynthesis Research Center of the Institute of Botany, and Drs. Yingchun Wang and Xiahe Huang from the Institute of Genetics and Developmental Biology, Chinese Academy of Sciences, for their excellent technical assistance with mass spectrometry analyses. We are also grateful to Mrs. Jialin Duan of the National Facility for Protein Science (NFPS) for instrument support and technical assistance during cryo-EM data collection. This work was supported in part by the National Key R&D Program of China (No. 2022YFC3401800), National Natural Science Foundation of China (32070264), Shandong Provincial Natural Science Foundation (ZR2019ZD48), the Strategic Priority Research Program of CAS (XDA26050402), the Science & Technology Specific Project in Agricultural High-tech Industrial Demonstration Area of the Yellow River Delta (2022SZX12), the Innovation Center for Academicians of Hainan Province, and the Specific Research Fund of the Innovation Center for Academicians of Hainan Province (No. YSPTZX202309). M.T.M. was supported in part by NASA Cooperative Agreement 80NSSC21M0355.

CONFLICTS OF INTEREST

The authors declare no conflicts of interest.

AUTHOR CONTRIBUTIONS

L.-J.Y. and C.-H.Q. conceived the project. C.-H.Q. and J.W. performed the sample preparation and characterization. F.-F. W. prepared cryo-EM grid and collected the cryo-EM data. G.-L.W. and C.-H.Q. processed the cryo-EM data and reconstructed the cryo-EM density map, built the structure model and refined the structure. C.-H.Q., G.-L.W., M.T.M., Y. K., Z.-Y. W.-O. and L.-J.Y. jointly wrote the manuscript. C.-H. Q., G.-L.W., F.-F.W., J.W., X.-P.W., M.-J.Z., F.M., M.T.M., Y. K., Z.-Y. W.-O. and L.-J.Y. contributed to the discussion of the results and the manuscript revision. All authors read and approved the contents of this paper.

Edited by: Jiamu Du, Southern University of Science and Technology, China

Received Nov. 10, 2023; **Accepted** Feb. 3, 2024

OO: OnlineOpen

REFERENCES

Adams, P.D., Afonine, P.V., Bunkoczi, G., Chen, V.B., Echols, N., Headd, J.J., Hung, L.W., Jain, S., Kapral, G.J., Grosse Kunstleve, R. W., et al. (2011). The Phenix software for automated determination of macromolecular structures. Methods **55:** 94–106.

Blankenship, R.E. (2021). *Molecular Mechanisms of Photosynthesis*. 3rd eds. John Wiley & Sons, Chichester.

Canniffe, D.P., and Hunter, C.N. (2014). Engineered biosynthesis of bacteriochlorophyll *b* in *Rhodobacter sphaeroides*. Biochim. Biophys. Acta **1837:** 1611–1616.

Cao, P., Bracun, L., Yamagata, A., Christianson, B.M., Negami, T., Zou, B., Terada, T., Canniffe, D.P., Shirouzu, M., and Li, M. (2022). Structural basis for the assembly and quinone transport mechanisms of the dimeric photosynthetic RC–LH1 supercomplex. Nat. Commun. **13:** 1–12.

Cogdell, R.J. (1985). Carotenoids in photosynthesis. Pure Appl. Chem. **57:** 723–728.

Cogdell, R.J., and Frank, H.A. (1987). How carotenoids function in photosynthetic bacteria. Biochim. Biophys. Acta **895:** 63–79.

Davis, C.M., Parkes-Loach, P.S., Cook, C.K., Meadows, K.A., Bandilla, M., Scheer, H., and Loach, P.A. (1996). Comparison of the structural requirements for bacteriochlorophyll binding in the core light-harvesting complexes of *Rhodospirillum rubrum* and *Rhodobacter sphaeroides* using reconstitution methodology with bacteriochlorophyll analogs. Biochemistry **35:** 3072–3084.

DeLano, W. (2004). *The Pymol Molecular Graphics System version 1.0*. Delano Scientific LLC, Palo Alto, CA.

Emsley, P., Lohkamp, B., Scott, W.G., and Cowtan, K. (2010). Features and development of Coot. Acta Crystallogr. D Biol. Crystallogr. **66:** 486–501.

Gardiner, A.T., Naydenova, K., Castro-Hartmann, P., Nguyen-Phan, T. C., Russo, C.J., Sader, K., Hunter, C.N., Cogdell, R.J., and Qian, P. (2021). The 2.4 Å cryo-EM structure of a heptameric light-harvesting 2 complex reveals two carotenoid energy transfer pathways. Sci. Adv. **7:** eabe4650.

Gardiner, A.T., Nguyen-Phan, T.C., and Cogdell, R.J. (2020). A comparative look at structural variation among RC-LH1 'Core' complexes present in anoxygenic phototrophic bacteria. Photosynth. Res. **145:** 83–96.

Hirose, M., Tsukatani, Y., Harada, J., and Tamiaki, H. (2022). Characterization of regioisomeric diterpenoid tails in bacteriochlorophylls produced by geranylgeranyl reductase from *Halorhodospira halochloris* and *Blastochloris viridis*. Photosynth. Res. **154:** 1–12.

Hitchcock, A., Swainsbury, D.J.K., and Hunter, C.N. (2023). Photosynthesis in the near infrared: The γ subunit of *Blastochloris viridis* LH1 redshifts absorption beyond 1,000 nm. Biochem. J. **480:** 455–460.

Imhoff, J.F., and Suling, J. (1996). The phylogenetic relationship among Ectothiorhodospiraceae: A reevaluation of their taxonomy on the basis of 16S rDNA analyses. Arch. Microbiol. **165:** 106–113.

Imhoff, J.F., and Trüper, H.G. (1977). *Ectothiorhodospira halochloris* sp. nov., a new extremely halophilic phototrophic bacterium containing bacteriochlorophyll *b*. Arch. Microbiol. **114:** 115–121.

Kimura, Y., Nakata, K., Nojima, S., Takenaka, S., Madigan, M.T., and Wang-Otomo, Z.-Y. (2022). Salt- and pH-dependent thermal stability of photocomplexes from extremophilic bacteriochlorophyll *b*-containing *Halorhodospira* species. Microorganisms **10:** 959.

Kimura, Y., Nojima, S., Nakata, K., Yamashita, T., Wang, X.P., Takenaka, S., Akimoto, S., Kobayashi, M., Madigan, M.T., Wang-Otomo, Z.Y., et al. (2021). Electrostatic charge controls the lowest LH1 Q_y transition energy in the triply extremophilic purple phototrophic bacterium, *Halorhodospira halochloris*. Biochim. Biophys. Acta, Bioenerg. **1862:** 148473.

Kimura, Y., Tani, K., Madigan, M.T., and Wang-Otomo, Z.-Y. (2023). Advances in the spectroscopic and structural characterization of core light-harvesting complexes from purple phototrophic bacteria. J. Phys. Chem. B **127:** 6–17.

Koepke, J., Hu, X., Muenke, C., Schulten, K., and Michel, H. (1996). The crystal structure of the light-harvesting complex II (B800-850) from *Rhodospirillum molischianum*. Structure **4:** 581–597.

Krogh, A., Larsson, B., von Heijne, G., and Sonnhammer, E.L. (2001). Predicting transmembrane protein topology with a hidden Markov model: Application to complete genomes. J. Mol. Biol. **305:** 567–580.

Liu, L.N., Bracun, L., and Li, M. (2024). Structural diversity and modularity of photosynthetic RC-LH1 complexes. Trends Microbiol. **32:** 38–52.

Mizoguchi, T., Isaji, M., Harada, J., Watabe, K., and Tamiaki, H. (2009). Structural determination of the Δ2, 10-phytadienyl substituent in the 17-propionate of bacteriochlorophyll-*b* from *Halorhodospira halochloris*. J. Porphyrins phthalocyanines **13:** 41–50.

Morosinotto, T., Breton, J., Bassi, R., and Croce, R. (2003). The nature of a chlorophyll ligand in Lhca proteins determines the far red fluorescence emission typical of photosystem I. J. Biol. Chem. **278:** 49223–49229.

Namoon, D., Rudling, N.M., and Canniffe, D.P. (2022). The role of the γ subunit in the photosystem of the lowest-energy phototrophs. Biochem. J. **479:** 2449–2463.

Parkes-Loach, P.S., Michalski, T.J., Bass, W.J., Smith, U., and Loach, P.A. (1990). Probing the bacteriochlorophyll binding site by reconstitution of the light-harvesting complex of *Rhodospirillum rubrum* with bacteriochlorophyll *a* analogs. Biochemistry **29:** 2951–2960.

Pettersen, E.F., Goddard, T.D., Huang, C.C., Couch, G.S., Greenblatt, D.M., Meng, E.C., and Ferrin, T.E. (2004). UCSF Chimera—A visualization system for exploratory research and analysis. J. Comput. Chem. **25:** 1605–1612.

Pettersen, E.F., Goddard, T.D., Huang, C.C., Meng, E.C., Couch, G.S., Croll, T.I., Morris, J.H., and Ferrin, T.E. (2021). UCSF ChimeraX: Structure visualization for researchers, educators, and developers. Protein Sci. **30:** 70–82.

Prince, S.M., Howard, T.D., Myles, D.A.A., Wilkinson, C., Papiz, M.Z., Freer, A.A., Cogdell, R.J., and Isaacs, N.W. (2003). Detergent structure in crystals of the integral membrane light-harvesting complex LH2 from *Rhodopseudomonas acidophila* strain 10050. J. Mol. Biol. **326:** 307–315.

Punjani, A., Rubinstein, J.L., Fleet, D.J., and Brubaker, M.A. (2017). cryoSPARC: Algorithms for rapid unsupervised cryo-EM structure determination. Nat. Methods **14:** 290–296.

Punjani, A., Zhang, H., and Fleet, D.J. (2020). Non-uniform refinement: Adaptive regularization improves single-particle cryo-EM reconstruction. Nat. Methods **17:** 1214–1221.

Qi, C.H., Wang, G.L., Wang, F.F., Xin, Y., Zou, M.J., Madigan, M.T., Wang-Otomo, Z.Y., Ma, F., and Yu, L.J. (2023). New insights on the photocomplex of *Roseiflexus castenholzii* revealed from comparisons of native and carotenoid-depleted complexes. J. Biol. Chem. **299:** 105057.

Qian, P., Croll, T.I., Hitchcock, A., Jackson, P.J., Salisbury, J.H., Castro-Hartmann, P., Sader, K., Swainsbury, D.J.K., and Hunter, C. N. (2021a). Cryo-EM structure of the dimeric *Rhodobacter sphaeroides* RC-LH1 core complex at 2.9 Å: The structural basis for dimerisation. Biochem. J. **478:** 3923–3937.

Qian, P., Croll, T.I., Swainsbury, D.J.K., Castro-Hartmann, P., Moriarty, N.W., Sader, K., and Hunter, C.N. (2021b). Cryo-EM structure of the *Rhodospirillum rubrum* RC–LH1 complex at 2.5 Å: The structural basis for dimerisation. Biochem. J. **478:** 3253–3263.

Qian, P., Gardiner, A.T., Simova, I., Naydenova, K., Croll, T.I., Jackson, P.J., Nupur, Kloz, M., Cubakova, P., Kuzma, M., et al. (2022). 2.4 Å structure of the double-ring *Gemmatimonas phototrophica* photosystem. Sci. Adv. **8:** eabk3139.

Qian, P., Siebert, C.A., Wang, P., Canniffe, D.P., and Hunter, C.N. (2018). Cryo-EM structure of the *Blastochloris viridis* LH1-RC complex at 2.9 Å. Nature **556:** 203–208.

Qian, P., Swainsbury, D.J.K., Croll, T.I., Castro-Hartmann, P., Divitini, G., Sader, K., and Hunter, C.N. (2021c). Cryo-EM structure of the

Rhodobacter sphaeroides light-harvesting 2 complex at 2.1 Å. Biochemistry **60:** 3302–3314.

Qian, P., Swainsbury, D.J.K., Croll, T.I., Salisbury, J.H., Martin, E.C., Jackson, P.J., Hitchcock, A., Castro-Hartmann, P., Sader, K., and Hunter, C.N. (2021d). Cryo-EM structure of the monomeric *Rhodobacter sphaeroides* RC-LH1 core complex at 2.5 Å. Biochem. J. **478:** 3775–3790.

Saga, Y., Yamashita, M., Masaoka, Y., Hidaka, T., Imanishi, M., Kimura, Y., and Nagasawa, Y. (2021). Excitation energy transfer from bacteriochlorophyll *b* in the B800 site to B850 bacteriochlorophyll *a* in light-harvesting complex 2. J. Phys. Chem. B **125:** 2009–2017.

Swainsbury, D.J., Faries, K.M., Niedzwiedzki, D.M., Martin, E.C., Flinders, A.J., Canniffe, D.P., Shen, G., Bryant, D.A., Kirmaier, C., and Holten, D. (2019). Engineering of B800 bacteriochlorophyll binding site specificity in the *Rhodobacter sphaeroides* LH2 antenna. Biochim. Biophys. Acta Bioenerg. **1860:** 209–223.

Swainsbury, D.J., Qian, P., Hitchcock, A., and Hunter, C.N. (2023). The structure and assembly of reaction centre-light-harvesting 1 complexes in photosynthetic bacteria. Biosci. Rep. **43:** BSR20220089.

Tani, K., Kanno, R., Ji, X.-C., Hall, M., Yu, L.-J., Kimura, Y., Madigan, M. T., Mizoguchi, A., Humbel, B.M., and Wang-Otomo, Z.-Y. (2021a). Cryo-EM structure of the photosynthetic LH1-RC complex from *Rhodospirillum rubrum*. Biochemistry **60:** 2483–2491.

Tani, K., Kanno, R., Kikuchi, R., Kawamura, S., Nagashima, K.V.P., Hall, M., Takahashi, A., Yu, L.J., Kimura, Y., Madigan, M.T., et al. (2022). Asymmetric structure of the native *Rhodobacter sphaeroides* dimeric LH1-RC complex. Nat. Commun. **13:** 1904.

Tani, K., Nagashima, K.V.P., Kanno, R., Kawamura, S., Kikuchi, R., Hall, M., Yu, L.-J., Kimura, Y., Madigan, M.T., Mizoguchi, A., et al. (2021b). A previously unrecognized membrane protein in the *Rhodobacter sphaeroides* LH1-RC photocomplex. Nat. Commun. **12:** 6300.

Tsukatani, Y., Hirose, Y., Harada, J., Yonekawa, C., and Tamiaki, H. (2019). Unusual features in the photosynthetic machinery of *Halorhodospira halochloris* DSM 1059 revealed by complete genome sequencing. Photosynth. Res. **140:** 311–319.

Wagner, T., and Raunser, S. (2020). The evolution of SPHIRE-crYOLO particle picking and its application in automated cryo-EM processing workflows. Commun. Biol **3:** 61.

Waterhouse, A., Bertoni, M., Bienert, S., Studer, G., Tauriello, G., Gumienny, R., Heer, F.T., de Beer, T.A.P., Rempfer, C., Bordoli, L., et al. (2018). SWISS-MODEL: Homology modelling of protein structures and complexes. Nucleic Acids Res. **46:** W296–W303.

Xin, J., Shi, Y., Zhang, X., Yuan, X., Xin, Y., He, H., Shen, J., Blankenship, R.E., and Xu, X. (2023). Carotenoid assembly regulates quinone diffusion and the *Roseiflexus castenholzii* reaction center-light harvesting complex architecture. eLife **12:** e88951.

Xin, Y., Shi, Y., Niu, T., Wang, Q., Niu, W., Huang, X., Ding, W., Yang, L., Blankenship, R.E., Xu, X., et al. (2018). Cryo-EM structure of the RC-LH core complex from an early branching photosynthetic prokaryote. Nat. Commun. **9:** 1568.

Yu, L.J., Suga, M., Wang-Otomo, Z.Y., and Shen, J.R. (2018). Structure of photosynthetic LH1-RC supercomplex at 1.9 Å resolution. Nature **556:** 209–213.

Zhang, Y., Qi, C.-H., Yamano, N., Wang, P., Yu, L.-J., Wang-Otomo, Z.-Y., and Zhang, J.-P. (2022). Carotenoid single-molecular singlet fission and the photoprotection of a bacteriochlorophyll *b*-Type core light-harvesting antenna. J. Phys. Chem. Lett. **13:** 3534–3541.

Zivanov, J., Nakane, T., and Scheres, S.H.W. (2020). Estimation of high-order aberrations and anisotropic magnification from cryo-EM data sets in RELION-3.1. IUCrJ **7:** 253–267.

SUPPORTING INFORMATION

Additional Supporting Information may be found online in the supporting information tab for this article: http://onlinelibrary.wiley.com/doi/10.1111/jipb.13628/suppinfo

Figure S1. Cryo-EM densities and structural models of components in the *Halorhodospira halochloris* LH1–RC complex
Figure S2. Cryo-EM of the *Halorhodospira halochloris* LH1–RC complex
Figure S3. Structure determination of the *Halorhodospira halochloris* LH1–RC complex
Figure S4. Amino acid sequences of *Halorhodospira halochloris* LH1 α-, β-, and γ-polypeptides from the protein database (GCF_002356555.2)
Figure S5. Comparison of amino acid sequences of *Halorhodospira halochloris* LH1 with those of other phototrophic bacteria LH1 complexes
Figure S6. Structural comparison and interaction of the *Halorhodospira halochloris* LH1 multiple polypeptides
Figure S7. Structures of BChl *b*
Figure S8. Pigments analysis of LH1–RC complex of *Halorhodospira halochloris*
Figure S9. Surface charge distributions of the LH1–RC complex
Figure S10. MS/MS fragmentations of protein Q and protein G peptides
Figure S11. Amino acid sequences of the two small proteins G and Q and their transmembrane regions predicted by the membrane protein topology program TMHMM
Figure S12. Interaction of proteins Q and G with neighboring LH and RC in the complex
Table S1. Cryo-EM data collection, refinement and validation statistics